ACS Photonics

pubs.acs.org/journal/apchd5

Article

Structurally Unraveling the Photocarrier Behavior of Cu_2O/ZnO Heterojunction Photodetectors

Shen Zhong, Da Xiong, Binbin Zhang, Xiao Yang, Tao Yang, Guo Tian, Hongrui Zhang, Weiqing Yang, and Weili Deng*

Cite This: *ACS Photonics* 2022, 9, 268−274

Read Online

ACCESS | Metrics & More | Article Recommendations | Supporting Information

ABSTRACT: Photoelectric conversion in a semiconductor is the basis of photodetectors (PDs), so unraveling the photocarrier behavior is essential for designing and enhancing the performance of PDs. Herein, we experimentally uncover the generation and transport behavior of the photocarrier in the self-powered Cu_2O/ZnO heterojunction PDs. The thickness of the functional layer is proved to be a major factor in determining the photocarrier generation and transport, namely, the increase in the number of photocarriers with the prolongation of the functional layer, while the transport of the carrier is impeded by the increase in the internal defects and becomes the degrading factor. By tuning the length of the ZnO nanorods, the structurally designed PD exhibits high responsivity of 45.74 mA/W under 450 nm light illumination at 0 V bias, which is 5.75 times larger than that of the quasi-planar one. Moreover, the PD presents a fast response speed (rise time of 5.5 ms and decay time of 5.9 ms) and long-term stability, showing only 3% degradation of the photocurrent after 30 days in the air. This work provides a microscopic perspective of photocarrier behavior for understanding the internal photoelectric conversion mechanism of the p−n junction-based PDs, which could further promote the practical applications of high-efficiency self-powered photodetectors.

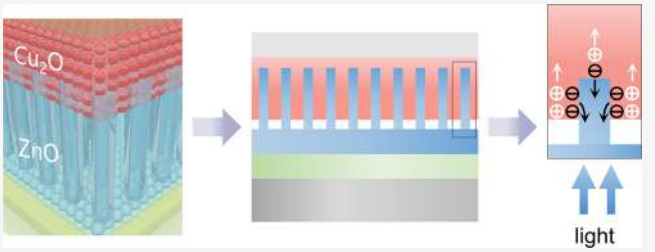

KEYWORDS: *ZnO nanorods, Cu_2O, length, defect, photodetector, photocarrier behavior*

INTRODUCTION

Photodetectors (PDs), which can convert light into electrical signals, are widely used in various applications, including optical imaging, telecommunications, and environmental surveillance.[1−6] Among various PDs based on different principles, self-powered PDs based on photovoltaic effect[7−9] have been a research hotspot as they can operate without an external power supply, which is advantageous for the development of wireless miniature optoelectronic devices. So far, as two of the most studied metal oxide materials, ZnO and Cu_2O represent preferred candidates to form a cost-effective, environment-friendly photovoltaic PD, which has been reported in many research studies.[10−12] In general, ZnO is an n-type semiconductor most commonly used in the ultraviolet (UV) PDs owing to its wide direct band gap (3.3 eV) and a high exciton binding energy (60 meV).[13−15] Compared with their thin-film counterparts, the one-dimensional (1D) ZnO nanorods (NRs) exhibit better optical and electrical properties, such as a larger aspect ratio and direct electron conduction, resulting in a greater electron diffusion coefficient of the ZnO NR array.[16−18] When forming a heterojunction with p-type Cu_2O, the separation of photogenerated electron−hole pairs is enhanced due to the appropriate position of their conduction and valence bands.[19] In addition, Cu_2O has a narrower band gap (1.9−2.2 eV) than that of ZnO,[20] which could broaden the device response spectrum to the visible region. To date, many efforts have been devoted to the fabrication of Cu_2O/ZnO-based PDs with enhanced photoelectric performance in the UV−vis region.[12,20−22]

Although the internal working mechanism of the p−n junction-based photodetectors has been revealed clearly, the behavior of the photocarrier still needs to be further investigated. Promisingly, a clearer explanation could be expected from the correlation between the photoelectric performance and the modulation of photocarrier behavior, such as photocarrier generation and transport. Herein, we investigated the influence of the length of ZnO NRs on the evolution of the photocarrier behavior of PDs to reveal the internal mechanism of the enhanced photoelectric performance. The behavior of the photocarrier was tuned by adjusting the length of ZnO NRs to modulate the final optical and electrical properties of Cu_2O/ZnO PDs. By structurally

Received: September 30, 2021
Published: January 5, 2022

https://doi.org/10.1021/acsphotonics.1c01490
ACS Photonics 2022, 9, 268−274

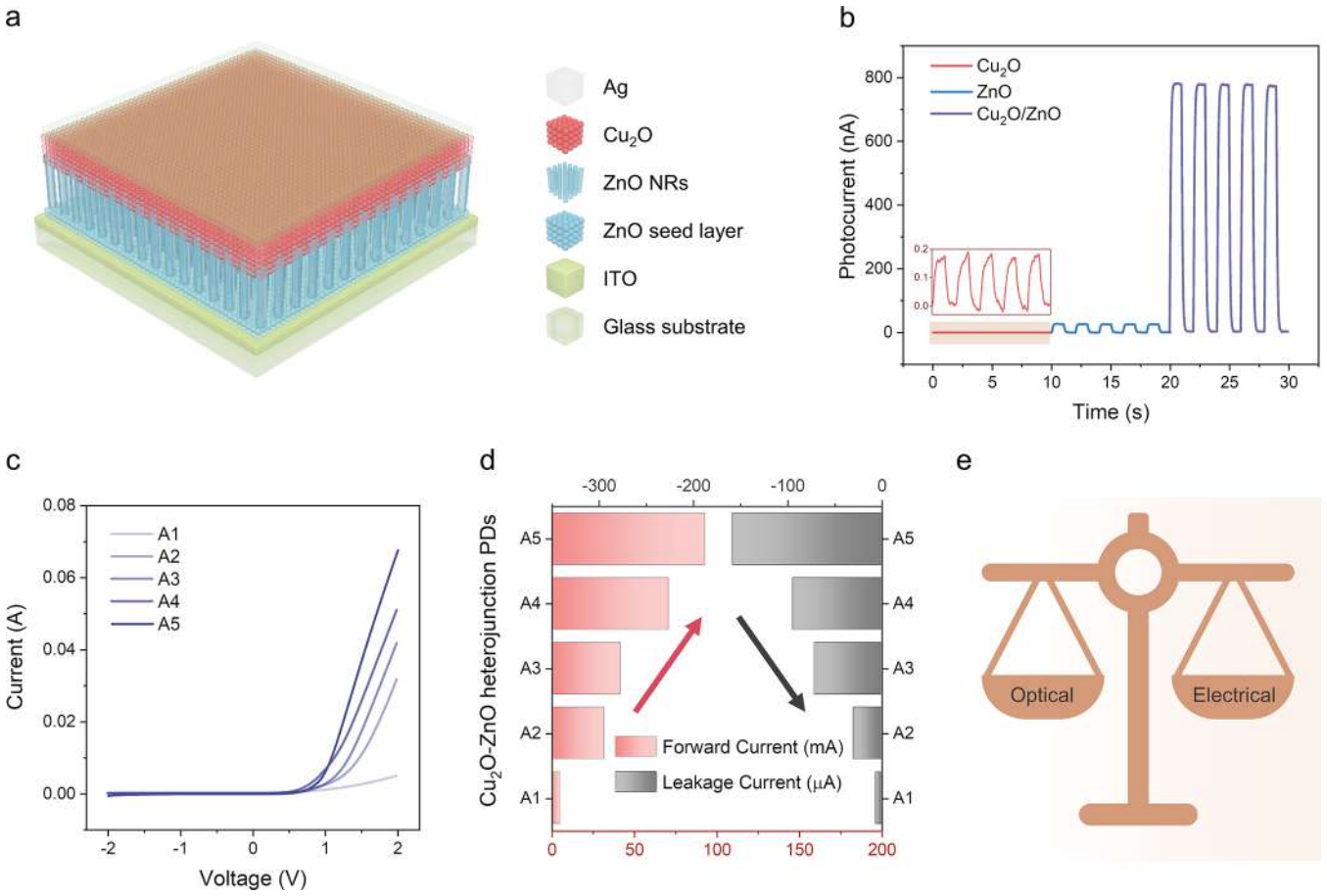

Figure 1. Schematic, characterization of the self-powered Cu_2O/ZnO heterojunction photodetector. (a) Schematic illustration of the structure of the Cu_2O/ZnO PD. (b) Comparison of the photoresponse behavior of the PDs based on Cu_2O, ZnO, and Cu_2O/ZnO heterojunction. (c) $I-V$ curves of the Cu_2O/ZnO heterojunction in the dark. (d) Forward currents at 2 V and reverse leakage currents at −2 V for Cu_2O/ZnO PDs with different ZnO NRs lengths. (e) Optimal balance between optical and electrical properties by tuning p−n junctions.

designing the PDs, the generation and transport of photocarriers were well-controlled, resulting in a 5.75 times enhancement of device photocurrent than that of the quasi-planar Cu_2O/ZnO PD. On this basis, the enhancement mechanism of Cu_2O/ZnO PDs was elucidated with the help of the energy band diagram. This work provides a simple strategy (tuning the material layer thickness) to control the device structure for optimal photoelectric performance and helps to understand the fundamental mechanism of heterojunction PDs, which could also be extended to other p−n junction-based photovoltaic devices.

RESULTS AND DISCUSSION

Figure 1a schematically depicts the structure of the fabricated Cu_2O/ZnO photodetector. A layer of ZnO seeds was deposited on the indium thin oxide (ITO)-coated glass substrate to provide nuclei for the synthesis of ZnO NRs, while the lattice mismatch between the ZnO NRs and the substrate can also be minimized.[23] Then, the hydrothermal method was adopted to grow ZnO NR array with various lengths on the seed layer.[24,25] Afterward, the Cu_2O layer was deposited on the ZnO NR array by the radio-frequency (RF) magnetron sputtering method. Finally, the Ag layer was deposited as an electrode by direct current (DC) sputtering. On this basis, when the light was incident from the ITO-coated glass side, the photocurrents converted from the optical signals can be detected with the help of a low-noise current preamplifier.

The typical photoelectric performance of the device with different structures under the same light conditions, including the single Cu_2O layer, the single ZnO NR array, and the Cu_2O/ZnO heterojunction, is demonstrated in Figure 1b. Apparently, the PD based on the p-type Cu_2O/n-type ZnO junction exhibits optimal performance, with photocurrents enhanced by a factor of 30 or 5000 over a single ZnO or Cu_2O-based PD (under 450 nm light illumination at 0 V). To further investigate the performance of Cu_2O/ZnO PD, photodetectors with different lengths of ZnO NRs were constructed by varying the growth time of ZnO NRs. Devices A1, A2, A3, A4, and A5 represent the PDs with different ZnO NRs lengths of 0.04, 0.18, 1.65, 1.11, and 1.52 μm, respectively (covered by a layer of Cu_2O with a length of 0.16 μm). From the $I-V$ curves of the Cu_2O/ZnO PDs in the dark (Figure 1c), it is clear that all of the as-fabricated PDs with different structural parameters show typical rectification behavior, indicating the good formation of p-type Cu_2O/n-type ZnO heterojunctions. As shown in Figure 1d, both the forward current and leakage current rise as the ZnO NRs lengthen. The longer the ZnO NRs, the larger the PD forward dark current (at 2 V bias), implying a larger heterojunction area, which is supposed to be beneficial for the light absorption and the separation of excitons, generating more electrons and

https://doi.org/10.1021/acsphotonics.1c01490
ACS Photonics 2022, 9, 268−274

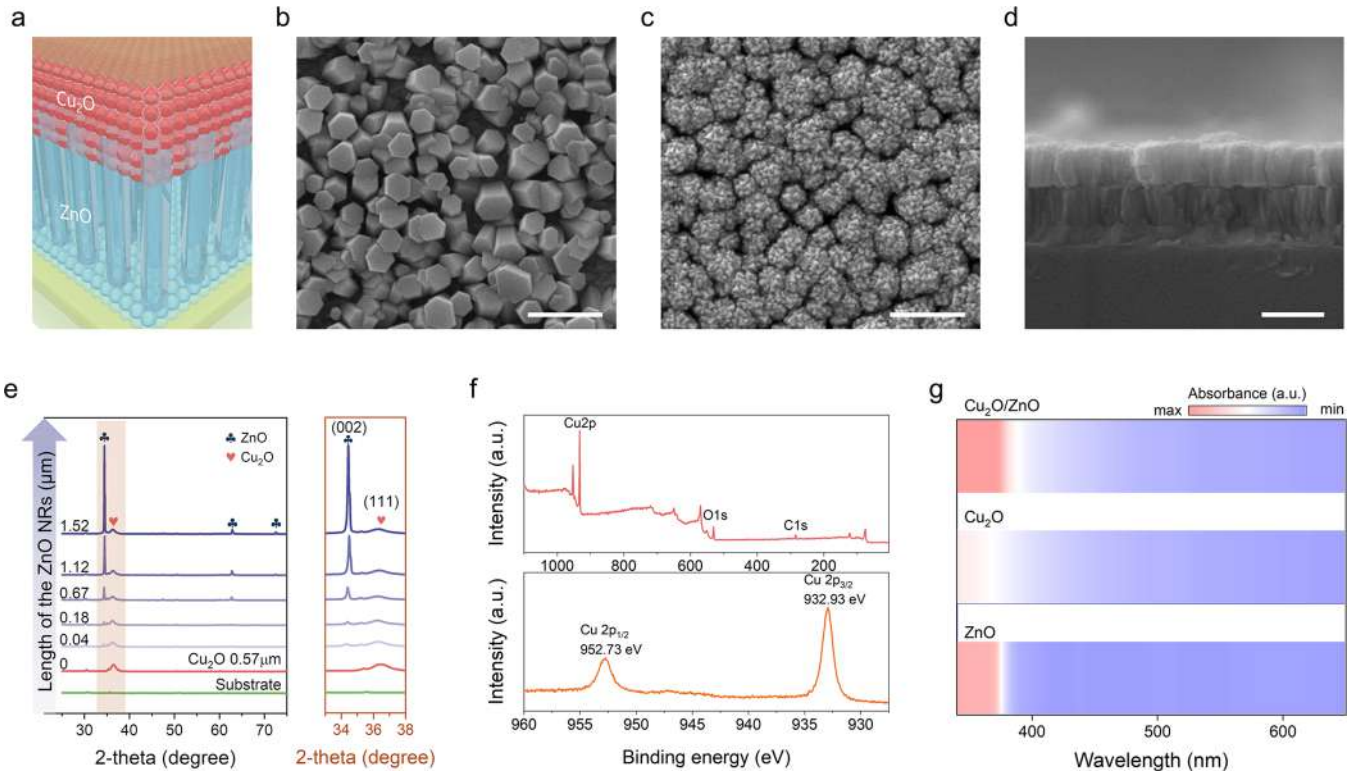

Figure 2. Characterization of the Cu_2O/ZnO heterojunction. (a) Schematic illustration of the Cu_2O/ZnO heterojunction. (b) Top view of ZnO NR array. (c) Top view of Cu_2O/ZnO nanorods, (d) Cross-sectional SEM image of the Cu_2O/ZnO heterojunction, all scale bars are 500 nm. (e) X-ray diffraction (XRD) patterns of the Cu_2O/ZnO heterojunction of different ZnO NR lengths. (f) X-ray photoelectron spectroscopy (XPS) survey spectrum of the Cu_2O/ZnO heterojunction and the core-level spectrum of Cu 2p in Cu_2O. (g) Absorbance spectra of the ZnO, Cu_2O, and Cu_2O/ZnO layers.

holes.[26,27] Meanwhile, the reverse leakage current (at −2 V bias) also increased when the ZnO NRs get longer, suggesting more defects acting as carrier recombination centers that hinder carrier transport.[28] Therefore, optimizing the ZnO NRs length is crucial to achieving a compromise between the optical and electrical properties of Cu_2O/ZnO PDs (Figure 1e).

An enlarged view of the Cu_2O/ZnO heterojunction is shown in Figure 2a, and this structure is further verified by surface and cross-sectional scanning electron microscopy (SEM) images. From the top-view SEM image of the ZnO NR array (Figure 2b), a regular hexagonal cross section of ZnO can be observed, implying the relatively high quality of the synthesized ZnO NR array. Cu_2O particles were evenly distributed on the surface of ZnO NRs and wrapped around the top of the nanorods (Figure 2c). Moreover, it can be seen from the cross-sectional image of the Cu_2O/ZnO heterojunction (Figure 2d) that the interlayer boundary between the Cu_2O and ZnO NRs is almost indistinguishable, as the Cu_2O particles were successfully sputtered into the gaps between the ZnO NRs, thus forming a quasi-core−shell structure that enhances the photon absorption and facilitates the separation of excitons. To verify this conjecture, the Cu_2O/ZnO heterojunction with different thicknesses have been prepared by regulating the synthesis time, as shown in Figure S1. Notably, in the case of longer ZnO NR array PDs, most of the Cu_2O particles could only be concentrated at the top of the ZnO NRs due to the increased diameter and the inevitable slight tilting of nanorods, forming a partial core−shell structure. In the case of the same length of ZnO NRs, the core−shell structure at the top of the nanorods became less obvious with the increase in the Cu_2O thickness, suggesting that the device structure varied with different lengths/thicknesses of ZnO/Cu_2O (Figures S2 and S3).

The Cu_2O/ZnO heterojunctions with varying lengths of ZnO NRs are investigated by XRD measurements (Figure 2e). The intense diffraction peak (002) implies that the ZnO NRs synthesized by the hydrothermal method have a wurtzite structure (PDF 36-1451) and grow along the +*c*-axis. As demonstrated in the enlarged view on the right, the longer the ZnO nanorods, the stronger the (002) peak (with a constant 0.57 μm Cu_2O layer), indicating that the oriented nanorods were obtained. The main lattice plane of Cu_2O is (111), which suggests a good orientation of Cu_2O prepared by RF magnetron sputtering. Owing to the small lattice mismatch between ZnO(002) and Cu_2O(111), the excessive interfacial states are suppressed to a certain extent and the influence of interfacial defects on the subsequent experiment could be reduced.[29,30] To further confirm the chemical state of the Cu element, the fabricated film was analyzed by XPS measurements (Figure 2f). The core-level spectrum of Cu 2p in Cu_2O shows that the Cu $2p_{3/2}$ and Cu $2p_{1/2}$ spin−orbital photoelectrons are located at 932.93 and 952.73 eV, respectively. Such results are consistent with previously reported Cu_2O values, indicating that the fabricated layer is Cu_2O rather than CuO or Cu.[19,31,32]

Figure 2g presents the absorbance spectra of the ZnO layer (0.18 μm NR array), the Cu_2O layer (0.16 μm), and the Cu_2O/ZnO heterojunction (0.18 μm ZnO NR array, 0.16 μm Cu_2O layer) based on the ITO-coated glass substrate. Apparently, ZnO NRs exhibit strong absorption under UV illumination (below 380 nm, the red zone) while there is

https://doi.org/10.1021/acsphotonics.1c01490
ACS Photonics 2022, 9, 268−274

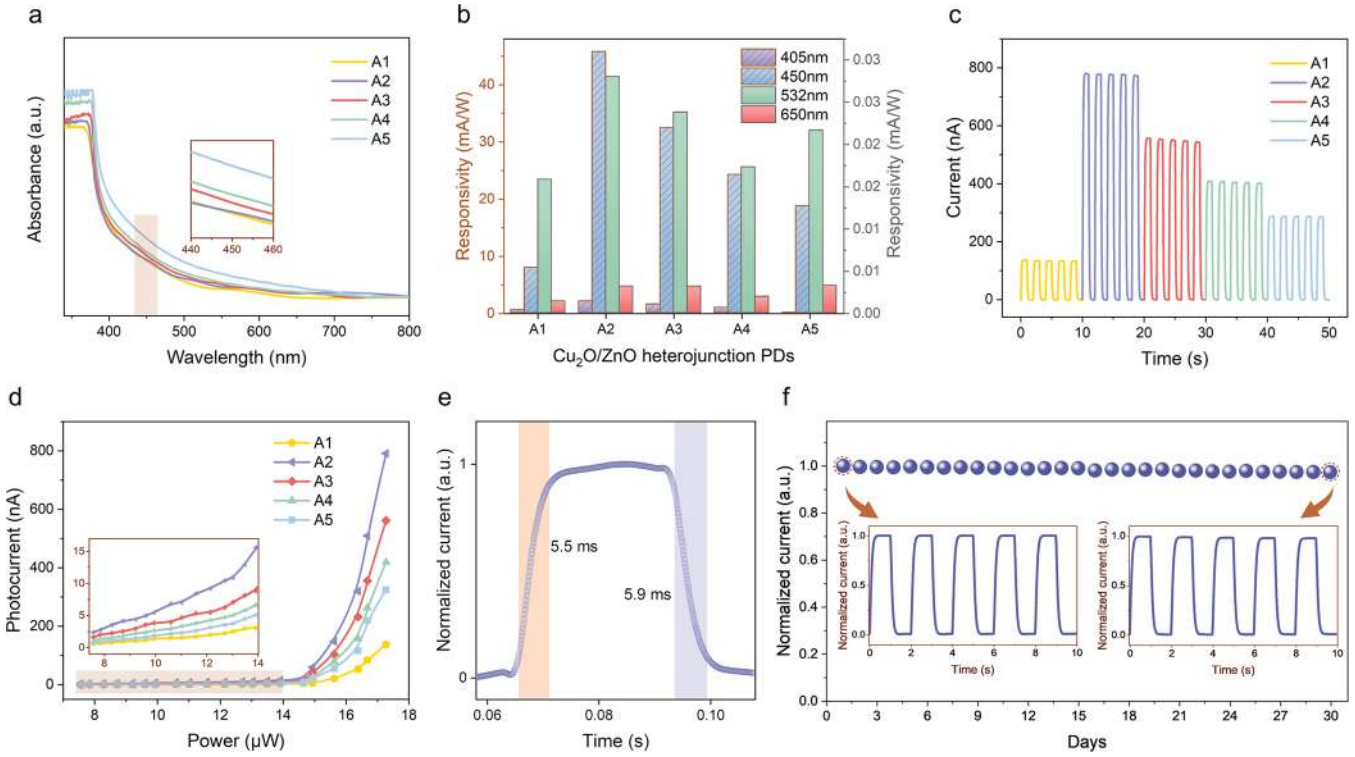

Figure 3. Optical and electrical performance of Cu_2O/ZnO heterojunction PDs. (a) Optical absorbance spectra of Cu_2O/ZnO heterojunctions. (b) Photoresponse behavior of the PDs under different wavelength illumination. (c) Comparison of the photoresponse behavior of the PDs without bias under 450 nm (17.27 μW) illumination. (d) Photoresponse of the PDs under different light powers (450 nm). (e) Response time of the fabricated device A2. (f) Normalized I–t curves of the device A2 for 30 days in the air.

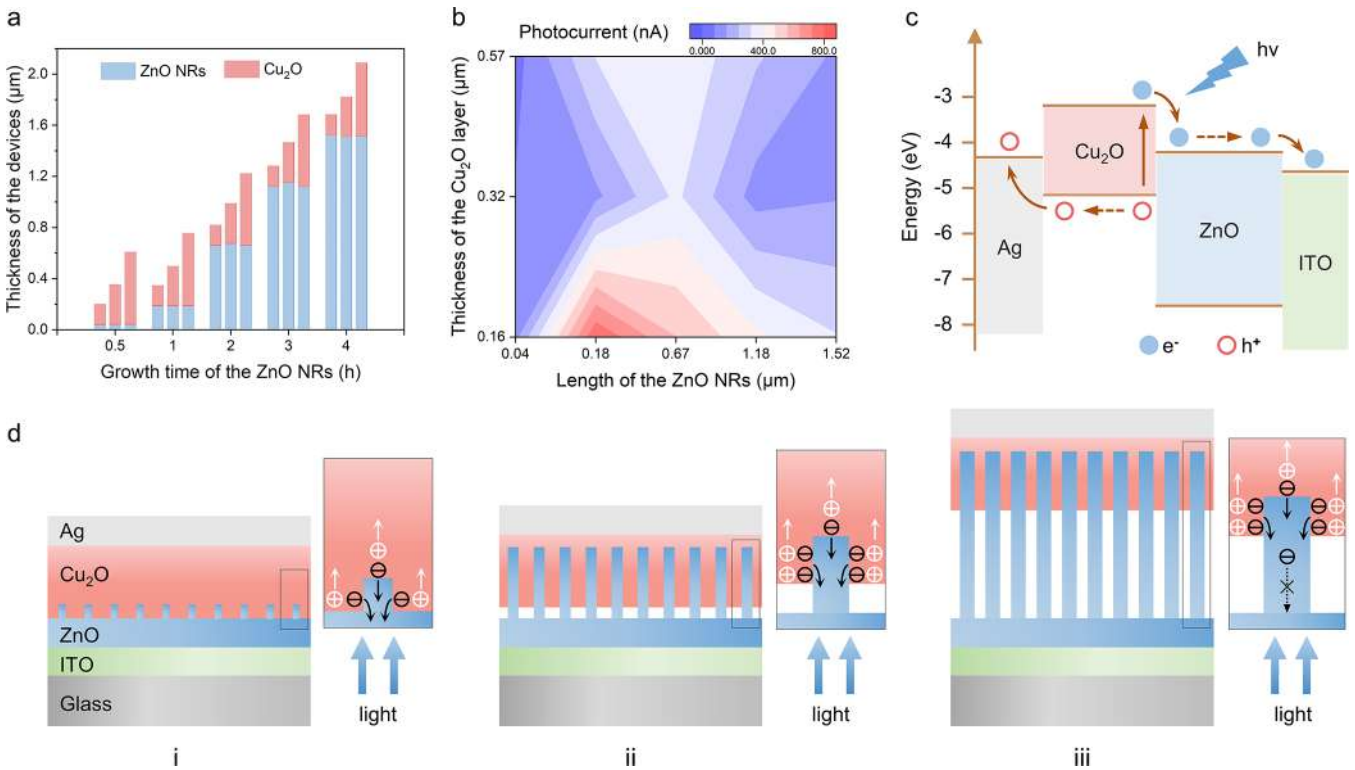

Figure 4. Working mechanism of the Cu_2O/ZnO heterojunction PD. (a) Overall relationship between the ZnO growth time/Cu_2O sputtering time and the heterojunction thickness. (b) Photocurrent of PDs with different ZnO NRs lengths and Cu_2O thicknesses. (c) Energy band diagram of the Cu_2O/ZnO heterojunction PDs. (d) Schematic of structure and photocarrier transportation mechanism of the Cu_2O/ZnO heterojunction PDs.

https://doi.org/10.1021/acsphotonics.1c01490
ACS Photonics 2022, 9, 268–274

almost no absorption in the visible region. In the meantime, Cu_2O expands the absorption to the visible region with an absorption edge around 650 nm (Figure S4). Then, when bonded together, the Cu_2O/ZnO heterojunction demonstrates stronger absorption in both UV and visible regions, suggesting that the p−n junction possesses stronger UV−vis absorption compared to a single ZnO or Cu_2O layer.

From the total optical absorbance spectra plot, it is clear that the UV−vis absorption intensity of the Cu_2O/ZnO heterojunction increased as the ZnO NRs grew longer (from A1 to A5) due to the enhancement of surface diffuse scattering in longer ZnO NRs[26] (Figure 3a). The enhancement of the visible-light absorption could be attributed to the augment of defects in longer ZnO NRs, as electrons could be excited to defect levels below the conduction band by photons with less energy than the ZnO band gap.[24] To some extent, the enhanced optical absorption due to the rise of defects is beneficial for the improvement of photoelectric performance. On this basis, the photoelectric performance of Cu_2O/ZnO PDs under visible-light illumination was further investigated. As shown in Figure 3b, a series of visible-light lasers of 405, 450, 532, and 650 nm were used for the measurement. It can be found that the performance of almost all devices shows a tendency to increase first and then decrease with the increasing length of ZnO NRs. Because of the relatively low absorption of the Cu_2O/ZnO heterojunction under 532 and 650 nm light illumination, the corresponding responsivities were slightly irregular. The device responsivity reaches a maximum of 45.74 mA W^{-1} at the optimal ZnO NRs length of 0.18 μm (device A2) under 450 nm light illumination, along with the highest photocurrent of up to 790 nA (Figure 3c). This phenomenon could be related to the balance between the optical and electrical properties of the Cu_2O/ZnO heterojunction. In detail, the increase in the ZnO NR length enhances the light absorption and induces more photocarriers, which promote the output photocurrent. Meanwhile, the defects acting as photocarrier traps also increase with the increase in the ZnO NR length, which impairs the final output. As a result, the photocurrent tends to rise and fall.

Furthermore, the influence of illumination density on the PDs was also studied (450 nm light illumination in Figure 3d, other wavelength illumination in Figure S5). By changing the signal voltage, the light power increased from 7.57 to 17.27 μW. The photocurrent of devices A1−A5 increased with the increment of the light power due to a higher probability of photon absorption by individual electrons in the presence of stronger light. Figure 3e shows the response time of device A2, which is composed of the rise and decay time, defined as the time required for the signal to vary between 10% and 90% of its peak value. In general, the p−n junction-based photodetectors have a shorter response time than that of the photoconductive detectors due to the built-in electric field in the heterojunction.[33] In this work, the rise time and decay time of the self-powered Cu_2O/ZnO PD were measured to be 5.5 and 5.9 ms, respectively. Moreover, owing to the intrinsic stability of the inorganic oxide, the Cu_2O/ZnO PD maintained 97% of the photoresponse current after 30 days (under 450 nm at 17.27 mW), showing a strong reproducibility for further applications (Figure 3f).

As aforementioned, Cu_2O/ZnO PDs with different lengths can be fabricated by adjusting the synthesis time of material layers. The specific length statistics of the as-prepared PDs are shown in Figure 4a. The PDs consisting of ZnO NRs with different lengths (0.04, 0.18, 1.67, 1.18, and 1.52 μm) and Cu_2O layers with different thicknesses (0.16, 0.32, and 0.57 μm) were prepared to further investigate their photoelectric performance. As a result, the photocurrent increases and then decreases when the thickness of the Cu_2O layer keeps constant and the length of the ZnO NRs increases under 450 nm light illumination at 0 V bias, as depicted in Figure 4b. Notably, the overall photoresponse of PDs with a thinner Cu_2O layer is better than that with a thicker Cu_2O layer, which could be attributed to more defects hindering the hole transport in the thicker Cu_2O layer.

To better explain the working mechanism of the Cu_2O/ZnO heterojunction PDs, the energy band diagram is adopted to describe the photocarrier behavior of the device, as illustrated in Figure 4c. The relative energy level difference between ZnO and Cu_2O generates the built-in electric field. Under 450 nm light, as Cu_2O is the main light-absorbing material, electron−hole pairs are generated on the Cu_2O side, near the Cu_2O/ZnO interface. Then, the electron−hole pairs are efficiently separated due to the existence of the built-in electric field. Electrons migrate from Cu_2O to ZnO and then to the ITO electrode, while holes move from Cu_2O to the Ag electrode. The photovoltaic current is induced when the electrons and holes are successfully collected by the ITO and Ag electrodes. Therefore, an above-band-gap light detection without an external bias was enabled by this photovoltaic effect.

In addition, the relationship between the ZnO NRs length and the photoelectric performance of the Cu_2O/ZnO PD is further analyzed graphically, as depicted in Figure 4d. Keeping the thickness of the Cu_2O layer constant, (i) when ZnO NRs are too short, the contact area of Cu_2O/ZnO is so limited that there is inadequate photon absorption at the interface of Cu_2O/ZnO, resulting in insufficient photogenerated electron−hole pairs and thus a poor photocurrent. (ii) With a proper ZnO NRs length, a quasi-core−shell structure could be constructed. Due to the stronger light-trapping effect and a larger p−n junction area, the photon absorption could be enhanced and more photocarriers are generated. Simultaneously, the Cu_2O shell layer surrounding the ZnO NRs reduces surface states by surface passivation and promotes the separation of excitons in the depletion layer. Such a structure reduces the carrier traveling distance and thus decreases the probability of carrier recombination during the carrier transport, ensuring adequate carrier collection and thus large photocurrent.[21,34,35] (iii) When ZnO NRs are much longer, more adequate light absorption can be ensured, but their internal and surface defects also increase. These defects can act as trapping centers for photocarriers, increasing the possibility of the electron−hole recombination and impeding electron transfer to the ITO electrode, thus greatly reducing the total photocurrent.[36,37] Therefore, the photoelectric performance of the Cu_2O/ZnO photodetector can be optimized by regulating the photocarrier behavior (generation and recombination) by adjusting the lengths of ZnO NRs.

CONCLUSIONS

In summary, the photocarrier behavior of the Cu_2O/ZnO heterojunction PDs was experimentally revealed by adjusting the lengths of the functional layers. It is found that the device photocurrent enhanced with the increasing length of ZnO NRs from 0.04 to 0.18 μm and then decreased sharply in longer ZnO NRs from 0.18 to 1.52 μm. At the optimal functional layer thickness (0.18 μm for ZnO and 0.16 μm for Cu_2O), the

https://doi.org/10.1021/acsphotonics.1c01490
ACS Photonics 2022, 9, 268−274

PD exhibits the responsivity of up to 45.74 mA W^{-1} and a fast response around 11.4 ms under 450 nm light illumination without a bias voltage. The stronger light-trapping effect promotes the generation of photocarriers in PD with relatively short ZnO NRs, while more surface and bulk defects in longer ZnO NRs impede the carrier transport, thus greatly reducing the photocurrent of the device. In the future, such a core−shell structure with larger space between the ZnO NRs holds the promise for high-performance Cu_2O/ZnO or other p−n junction PDs. To achieve an optimal photoelectric performance of p−n junction PDs, enhancement of light absorption and suppression of defect trap centers should be considered at the same time.

EXPERIMENTAL SECTION

Preparation of the Cu_2O/ZnO Heterojunction PDs. ZnO NRs were synthesized by the two-step hydrothermal method. First, the ZnO seed layer was deposited on an ITO-coated glass substrate by the radio-frequency (RF) magnetron sputtering to provide nuclei for the synthesis of ZnO NRs. The ZnO seed layer/ITO glass was then immersed into the mixed 0.1 M growth solution (zinc nitrate ($Zn(NO_3)_2{\cdot}6H_2O$) and hexamethylenetetramine (HMTA)) to synthesize ZnO nanorods at 85 °C. ZnO NR arrays of different lengths were obtained by changing the reaction time (0.5, 1, 2, 3, and 4 h). Then, the samples were washed with deionized water and annealed at 200 °C for 2 h. Next, the Cu_2O layer was deposited on the as-synthesized ZnO nanorods by RF magnetron sputtering for 0.5, 1, and 2 h. Finally, a thin layer of silver (Ag) was subsequently sputtered on the Cu_2O layer as the top electrode.

Characterization. A field emission scanning electron microscope was used to characterize the morphology of the Cu_2O/ZnO heterojunctions (FESEM JSM7800F). X-ray diffraction (XRD X'pert Powder) with a Cu Kα radiation at 40 kV and 40 mA was performed to evaluate the crystal structure of the samples. The optical absorption spectra of the samples were recorded with a UV−vis−NIR spectrophotometer (UV2310 II). The current−voltage (I−V) characteristics of the fabricated p-Cu_2O/n-ZnO heterojunction devices were measured by a Keithley 4200 source-measure unit. The electric signals were measured by a low-noise current preamplifier (Stanford SR 570). The lasers (405, 450, 532, and 650 nm) were used for the illumination of Cu_2O/ZnO heterojunction PDs.

ASSOCIATED CONTENT

Supporting Information

The Supporting Information is available free of charge at https://pubs.acs.org/doi/10.1021/acsphotonics.1c01490.

Experimental details of the preparation of the Cu_2O/ZnO photodetector; additional SEM images of Cu_2O and the Cu_2O/ZnO heterojunction; absorbance spectra of the material layer and Cu_2O/ZnO heterojunction; and details of the photoelectric performance of all of the fabricated photodetectors (PDF)

AUTHOR INFORMATION

Corresponding Author

Weili Deng − *Key Laboratory of Advanced Technologies of Materials (Ministry of Education), School of Materials Science and Engineering, Southwest Jiaotong University, Chengdu 610031, P. R. China;* orcid.org/0000-0003-1427-534X; Email: weili1812@swjtu.edu.cn

Authors

Shen Zhong − *Key Laboratory of Advanced Technologies of Materials (Ministry of Education), School of Materials Science and Engineering, Southwest Jiaotong University, Chengdu 610031, P. R. China*

Da Xiong − *Key Laboratory of Advanced Technologies of Materials (Ministry of Education), School of Materials Science and Engineering, Southwest Jiaotong University, Chengdu 610031, P. R. China*

Binbin Zhang − *Key Laboratory of Advanced Technologies of Materials (Ministry of Education), School of Materials Science and Engineering, Southwest Jiaotong University, Chengdu 610031, P. R. China*

Xiao Yang − *School of Electrical Engineering, Southwest Jiaotong University, Chengdu 610031, P. R. China*

Tao Yang − *Key Laboratory of Advanced Technologies of Materials (Ministry of Education), School of Materials Science and Engineering, Southwest Jiaotong University, Chengdu 610031, P. R. China*

Guo Tian − *Key Laboratory of Advanced Technologies of Materials (Ministry of Education), School of Materials Science and Engineering, Southwest Jiaotong University, Chengdu 610031, P. R. China*

Hongrui Zhang − *Key Laboratory of Advanced Technologies of Materials (Ministry of Education), School of Materials Science and Engineering, Southwest Jiaotong University, Chengdu 610031, P. R. China*

Weiqing Yang − *Key Laboratory of Advanced Technologies of Materials (Ministry of Education), School of Materials Science and Engineering, Southwest Jiaotong University, Chengdu 610031, P. R. China;* orcid.org/0000-0001-8828-9862

Complete contact information is available at: https://pubs.acs.org/10.1021/acsphotonics.1c01490

Notes

The authors declare no competing financial interest.

ACKNOWLEDGMENTS

This work was financially supported by the National Natural Science Foundation of China (No. 61801403), the Sichuan Province Foundation for Distinguished Young Team (No. 20CXTD0106), the Sichuan Science and Technology Program (No. 2020YFG0370), and the Cultivation Project of Basic Research (No. 2682021ZTPY004). The authors would like to express their gratitude to the Analytical and Testing Center of Southwest Jiaotong University for their assistance with the SEM and XRD measurements.

REFERENCES

(1) Zhuge, F.; Zheng, Z.; Luo, P.; Lv, L.; Huang, Y.; Li, H.; Zhai, T. Nanostructured Materials and Architectures for Advanced Infrared Photodetection. *Adv. Mater. Technol.* **2017**, *2*, No. 1700005.

(2) Chen, S.; Lou, Z.; Chen, D.; Shen, G. An Artificial Flexible Visual Memory System Based on an UV-Motivated Memristor. *Adv. Mater.* **2018**, *30*, No. 1705400.

(3) Rein, M.; Favrod, V. D.; Hou, C.; Khudiyev, T.; Stolyarov, A.; Cox, J.; Chung, C. C.; Chhav, C.; Ellis, M.; Joannopoulos, J.; Fink, Y. Diode Fibres for Fabric-Based Optical Communications. *Nature* **2018**, *560*, 214−218.

(4) Zeng, J.; Meng, C.; Li, X.; Wu, Y.; Liu, S.; Zhou, H.; Wang, H.; Zeng, H. Interfacial-Tunneling-Effect-Enhanced $CsPbBr_3$ Photodetectors Featuring High Detectivity and Stability. *Adv. Funct. Mater.* **2019**, *29*, No. 1904461.
(5) Li, L.; Chen, H.; Fang, Z.; Meng, X.; Zuo, C.; Lv, M.; Tian, Y.; Fang, Y.; Xiao, Z.; Shan, C.; Xiao, Z.; Jin, Z.; Shen, G.; Shen, L.; Ding, L. An Electrically Modulated Single-Color/Dual-Color Imaging Photodetector. *Adv. Mater.* **2020**, *32*, No. 1907257.
(6) Zhou, W.; Shang, Y.; de Arquer, F. P. G.; Xu, K.; Wang, R.; Luo, S.; Xiao, X.; Zhou, X.; Huang, R.; Sargent, E. H.; Ning, Z. Solution-Processed Upconversion Photodetectors Based on Quantum Dots. *Nat. Electron.* **2020**, *3*, 251−258.
(7) Hatch, S. M.; Briscoe, J.; Dunn, S. A Self-Powered ZnO-Nanorod/CuSCN UV Photodetector Exhibiting Rapid Response. *Adv. Mater.* **2013**, *25*, 867−871.
(8) Bie, Y. Q.; Liao, Z. M.; Zhang, H. Z.; Li, G. R.; Ye, Y.; Zhou, Y. B.; Xu, J.; Qin, Z. X.; Dai, L.; Yu, D. P. Self-Powered, Ultrafast, Visible-Blind UV Detection and Optical Logical Operation Based on ZnO/GaN Nanoscale p-n Junctions. *Adv. Mater.* **2011**, *23*, 649−653.
(9) Tian, W.; Wang, Y.; Chen, L.; Li, L. Self-Powered Nanoscale Photodetectors. *Small* **2017**, *13*, No. 1701848.
(10) Deo, M.; Mujawar, S.; Game, O.; Yengantiwar, A.; Banpurkar, A.; Kulkarni, S.; Jog, J.; Ogale, S. Strong Photo-Response in a Flip-Chip Nanowire p-Cu_2O/n-ZnO Junction. *Nanoscale* **2011**, *3*, 4706−4712.
(11) Lin, P.; Chen, X.; Yan, X.; Zhang, Z.; Yuan, H.; Li, P.; Zhao, Y.; Zhang, Y. Enhanced Photoresponse of Cu_2O/ZnO Heterojunction with Piezo-Modulated Interface Engineering. *Nano Res.* **2014**, *7*, 860−868.
(12) De Melo, C.; Jullien, M.; Battie, Y.; Naciri, A. E.; Ghanbaja, J.; Montaigne, F.; Pierson, J.-F.; Rigoni, F.; Almqvist, N.; Vomiero, A.; Migot, S.; Muecklich, F.; Honwat, D. Semi-Transparent p-Cu_2O/n-ZnO Nanoscale-Film Heterojunctions for Photodetection and Photovoltaic Applications. *ACS Appl. Nano Mater.* **2019**, *2*, 4358−4366.
(13) Guo, F.; Yang, B.; Yuan, Y.; Xiao, Z.; Dong, Q.; Bi, Y.; Huang, J. A Nanocomposite Ultraviolet Photodetector Based on Interfacial Trap-Controlled Charge Injection. *Nat. Nanotechnol.* **2012**, *7*, 798−802.
(14) Zheng, Z.; Gan, L.; Zhang, J.; Zhuge, F.; Zhai, T. An Enhanced UV−Vis−NIR and Flexible Photodetector Based on Electrospun ZnO Nanowire Array/PbS Quantum Dots Film Heterostructure. *Adv. Sci.* **2017**, *4*, No. 1600316.
(15) Peng, W.; Wang, X.; Yu, R.; Dai, Y.; Zou, H.; Wang, A. C.; He, Y.; Wang, Z. L. Enhanced Performance of a Self-Powered Organic/Inorganic Photodetector by Pyro-Phototronic and Piezo-Phototronic Effects. *Adv. Mater.* **2017**, *29*, No. 1606698.
(16) Tian, Z. R.; Voigt, J. A.; Liu, J.; Mckenzie, B.; Mcdermott, M. J.; Rodriguez, M. A.; Konishi, H.; Xu, H. Complex and Oriented ZnO Nanostructures. *Nat. Mater.* **2003**, *2*, 821−826.
(17) Vayssieres, L. Growth of Arrayed Nanorods and Nanowires of ZnO from Aqueous Solutions. *Adv. Mater.* **2003**, *15*, 464−466.
(18) Sang, L.; Liao, M.; Sumiya, M. A Comprehensive Review of Semiconductor Ultraviolet Photodetectors: From Thin Film to One-Dimensional Nanostructures. *Sensors* **2013**, *13*, 10482−10518.
(19) Xiong, D.; Deng, W.; Tian, G.; Gao, Y.; Chu, X.; Yan, C.; Jin, L.; Su, Y.; Yan, W.; Yang, W. A Piezo-Phototronic Enhanced Serrate-Structured ZnO-Based Heterojunction Photodetector for Optical Communication. *Nanoscale* **2019**, *11*, 3021−3027.
(20) Bai, Z.; Zhang, Y. Self-Powered UV−Visible Photodetectors Based on ZnO/Cu_2O Nanowire/Electrolyte Heterojunctions. *J. Alloys Compd.* **2016**, *675*, 325−330.
(21) Ghamgosar, P.; Rigoni, F.; You, S.; Dobryden, I.; Kohan, M. G.; Pellegrino, A. L.; Concina, I.; Almqvist, N.; Malandrino, G.; Vomiero, A. ZnO-Cu_2O Core-Shell Nanowires as Stable and Fast Response Photodetectors. *Nano Energy* **2018**, *51*, 308−316.
(22) Lin, H. P.; Lin, P. Y.; Perng, D. C. Fast-Response and Self-Powered Cu_2O/ZnO Nanorods Heterojunction UV-Visible (570 nm) Photodetectors. *J. Electrochem. Soc.* **2020**, *167*, No. 067507.
(23) Guo, M.; Diao, P.; Cai, S. Hydrothermal Growth of Well-Aligned ZnO Nanorod Arrays: Dependence of Morphology and Alignment Ordering upon Preparing Conditions. *J. Solid State Chem.* **2005**, *178*, 1864−1873.
(24) Tam, K. H.; Cheung, C. K.; Leung, Y. H.; Djurišić, A. B.; Ling, C. C.; Beling, C. D.; Fung, S.; Kwok, W. M.; Chan, W. K.; Phillips, D. L.; Ding, L.; Ge, W. K. Defects in ZnO Nanorods Prepared by a Hydrothermal Method. *J. Phys. Chem. B* **2006**, *110*, 20865−20871.
(25) Xu, S.; Wang, Z. L. One-Dimensional ZnO Nanostructures: Solution Growth and Functional Properties. *Nano Res.* **2011**, *4*, 1013−1098.
(26) Musselman, K. P.; Wisnet, A.; Iza, D. C.; Hesse, H. C.; Scheu, C.; MacManus-Driscoll, J. L.; Schmidt-Mende, L. Strong Efficiency Improvements in Ultra-Low-Cost Inorganic Nanowire Solar Cells. *Adv. Mater.* **2010**, *22*, E254−E258.
(27) Chen, X.; Lin, P.; Yan, X.; Bai, Z.; Yuan, H.; Shen, Y.; Liu, Y.; Zhang, G.; Zhang, Z.; Zhang, Y. Three-Dimensional Ordered ZnO/Cu_2O Nanoheterojunctions for Efficient Metal−Oxide Solar Cells. *ACS Appl. Mater. Interfaces* **2015**, *7*, 3216−3223.
(28) Ke, N. H.; Trinh, L. T. T.; Phung, P. K.; Loan, P. T. K.; Tuan, D. A.; Truong, N. H.; Tran, C. V.; Hung, L. V. T. Changing the Thickness of Two Layers: i-ZnO Nanorods, p-Cu_2O and Its Influence on the Carriers Transport Mechanism of the p-Cu_2O/i-ZnO Nanorods/n-IGZO Heterojunction. *SpringerPlus* **2016**, *5*, No. 710.
(29) Izaki, M.; Shinagawa, T.; Mizuno, K. T.; Ida, Y.; Inaba, M.; Tasaka, A. Electrochemically Constructed p-Cu_2O/n-ZnO Heterojunction Diode for Photovoltaic Device. *J. Phys. D: Appl. Phys.* **2007**, *40*, 3326−3329.
(30) Jia, W.; Dong, H.; Zhao, J.; Dang, S.; Zhang, Z.; Li, T.; Liu, X.; Xu, B. P-Cu_2O/n-ZnO Heterojunction Fabricated by Hydrothermal Method. *Appl. Phys. A* **2012**, *109*, 751−756.
(31) Lalitha, K.; Sadanandam, G.; Kumari, V. D.; Subrahmanyam, M.; Sreedhar, B.; Hebalkar, N. Y. Highly Stabilized and Finely Dispersed Cu_2O/TiO_2: A Promising Visible Sensitive Photocatalyst for Continuous Production of Hydrogen from Glycerol: Water Mixtures. *J. Phys. Chem. C* **2010**, *114*, 22181−22189.
(32) Liu, X.; Du, H.; Wang, P.; Lim, T. T.; Sun, X. W. A High-Performance UV/Visible Photodetector of Cu_2O/ZnO Hybrid Nanofilms on SWNT-Based Flexible Conducting Substrates. *J. Mater. Chem. C* **2014**, *2*, 9536−9542.
(33) Qiu, Q.; Huang, Z. Photodetectors of 2D Materials from Ultraviolet to Terahertz Waves. *Adv. Mater.* **2021**, *33*, No. 2008126.
(34) Cui, J.; Gibson, U. J. A Simple Two-Step Electrodeposition of Cu_2O/ZnO Nanopillar Solar Cells. *J. Phys. Chem. C* **2010**, *114*, 6408−6412.
(35) Tsai, S. H.; Chang, H. C.; Wang, H. H.; Chen, S. Y.; Lin, C. A.; Chen, S. A.; Chueh, Y. L.; He, J. H. Significant Efficiency Enhancement of Hybrid Solar Cells Using Core−Shell Nanowire Geometry for Energy Harvesting. *ACS Nano* **2011**, *5*, 9501−9510.
(36) Wang, H. P.; He, J. H. Toward Highly Efficient Nanostructured Solar Cells Using Concurrent Electrical and Optical Design. *Adv. Energy Mater.* **2017**, *7*, No. 1602385.
(37) Sharma, S.; Sumathi, A.; Periasamy, C. Photodetection Properties of ZnO/Si Heterojunction Diode: A Simulation Study. *IETE Tech. Rev.* **2017**, *34*, 83−90.

https://doi.org/10.1021/acsphotonics.1c01490
ACS Photonics 2022, 9, 268−274